Journal of the European Ceramic Society 22 (2002) 279–288

www.elsevier.com/locate/jeurceramsoc

# Processing and properties of zirconium diboride-based composites

F. Monteverde, A. Bellosi*, S. Guicciardi

*CNR-IRTEC, Research Institute for Ceramics Technology, Via Granarolo 64, 48018 Faenza, Italy*

Received 11 January 2001; accepted 28 March 2001

**Abstract**

Two zirconium diboride-base composites were produced and characterised. The chosen starting compositions were: 55 wt.% $ZrB_2$ + 41 wt.%$TiB_2$ + 4 wt.% Ni and 83 wt.% $ZrB_2$ + 13 wt.% $B_4C$ + 4 wt.% Ni. The microstructure and properties of these composites were compared to those of a monolithic $ZrB_2$ + 4 wt.% Ni material. In all cases, metallic Ni as the sintering aid promoted the formation of the liquid phase which improved mass transfer mechanisms during sintering. From the powder mixture $ZrB_2$ + $TiB_2$, two solid solutions of Zr–Ti–B were obtained. In the case of the other mixture, $B_4C$ particles were dispersed in the $ZrB_2$ matrix. The composite materials have better mechanical properties than those of the monolithic $ZrB_2$ ceramic; in particular the fracture toughness and the flexural strength were almost doubled at room temperature. Long term oxidation tests indicated that the $ZrB_2$-based composites, particularly the composite containing $B_4C$ as the second phase, were more resistant to oxidation than the monolithic $ZrB_2$ due to the formation of surface oxide products which were protective against the complete degradation by oxidation observed for the $ZrB_2$ matrix material. 

*Keywords:* $B_4C$; Composites; Electrical properties; Mechanical properties; Thermal properties; $TiB_2$; $ZrB_2$

## 1. Introduction

Zirconium diboride ($ZrB_2$) ceramics have a high melting point, high hardness, high electrical conductivity, excellent corrosion resistance against molten iron and slags and superb thermal shock resistance. They constitute a class of promising materials for high temperature applications in several industrial sectors, like foundry or refractory industries. Like $TiB_2$, $ZrB_2$ is wetted by molten metals but is not attacked by them, making it a useful material for molten metal crucibles, thermowell tubes for steel refining and parts of electrical devices such as heaters and igniters.[1] Applications are also found in the aerospace industry: hypersonic re-entry vehicles, leading edges, nose caps, rocket nozzle inserts and air-augmented propulsion system components.[1–4]

To ensure that favourable properties are obtained, control of densification and microstructure is necessary because strength and corrosion resistance are adversely affected by porosity in sintered bodies. Due to the high melting point and high vapour pressure of the constituents, the sintering of $ZrB_2$ powders is rather difficult. Relatively high densities are achieved only by pressure-assisted sintering procedures at temperatures higher than 1900°C, i.e. temperatures exceeding 70% of the absolute melting temperature.[1,5] As with $TiB_2$ materials,[6] the introduction of sintering aids such as Fe, Ni, Co, W, C, WC improves the final density and allows a lower densification temperature,[1,7] increasing volume diffusion and retarding evaporation mechanisms. Attempts to densify $ZrB_2$ without sintering aids or with the addition of boron resulted in rather low final densities.[8] The properties of the dense materials then become strictly dependent on the starting powders and processing parameters as they determine microstructural features such as grain size, volume and chemistry of the secondary phases, etc.

As the reliability of $ZrB_2$-based materials for electrical and mechanical applications is limited by their poor properties of toughness, stress corrosion cracking and high temperature oxidation, many applications of these materials require the addition of a second reinforcing phase to form complex structures or alloying elements to form solid solutions.[9–17] Studies were made on ceramic composites containing $ZrB_2$ as a second reinforcing and electroconductive phase,[9–12,18–24] thanks to the low electrical resistivity of $ZrB_2$.[25–27] Among the advantages

* Corresponding author. Tel.: +39-546-699-759; fax: +39-546-46381.

*E-mail address:* bellosi@irtec1.irtec.bo.cnr.it (A. Bellosi).

0955-2219/01/$ - see front matter 
PII: S0955-2219(01)00284-9

of electroconductive monolithic or composite $ZrB_2$-based ceramics, the possibility of machining them by electrical discharge offers a powerful tool for the manufacture of complex shaped components.[26–29] Another critical aspect of refractory borides is their low thermal stability in air at high temperature, although several studies have shown the formation of a surface protective scale of borosilicate glasses.[3] Again, attempts were made to improve the oxidation resistance of $ZrB_2$-based materials, through the addition of appropriate additives.[9,20,30–32]

This work aims to highlight the microstructure and properties of two $ZrB_2$-based ceramic composites obtained from fine commercial $ZrB_2$ powders and the addition of $TiB_2$ or $B_4C$ as secondary phases. Microstructure, mechanical properties, electrical resistivity and oxidation resistance were evaluated and compared to those of monolithic $ZrB_2$.[33]

## 2. Experiments

$ZrB_2$, $TiB_2$ and $B_4C$ powders produced by H. C. Starck (Germany) were selected as raw materials.

Their main properties are summarised in Table 1: the chemical composition was supplied by the producer except the oxygen amounts which were determined by LECO. The specific surface areas were measured by the BET method while grain size and morphology were evaluated by SEM analyses. The particle shape of all the powders was irregular and mainly acicular, with a large grain size distribution.

Compositions of the two $ZrB_2$-based composites, of the monolithic material and the adopted parameters necessary to obtain high densities by hot pressing are shown in Table 2. A Ni powder was selected as a sintering aid for the monolithic and composite materials.

The powder batches were homogenised by wet mixing in ethanol using zirconia balls. The hot pressing cycles were carried out under vacuum using a BN-lined graphite die.

The microstructure was analysed by scanning electron microscopy and EDX analysis on polished and fracture surfaces. The crystalline phases were identified by X-ray diffraction analyses.

The following mechanical properties were measured: elastic modulus ($E$) by the resonance frequency method on $28\times8\times0.8$ mm$^3$ samples, 4-pt flexural strength ($\sigma$) on $25\times2.5\times2$ (length×width×thickness) mm$^3$ test bars, using an outer span of 40 mm and an inner span of 20 mm with a crosshead speed of 0.5 mm/min, from room temperature up to 1400°C; microhardness (HV1.0) by a Vickers indenter with an applied load 9.81 N; fracture toughness ($K_{IC}$) using two methods: (i) direct crack measurement (DCM)[34] with a load of 98.1 N, (ii) chevron notched beam method (CNB)[35] on $25\times2\times2.5$ (length×width×thickness) mm$^3$ bars with a machine crosshead speed of 0.05 mm/min.

The thermal expansion behaviour was tested in air up to 1400°C.

The electrical resistivity measurements were carried out by a four probe DC method at room temperature, inducing a current in bar specimens of $2\times2.5\times25$ mm$^3$. The current and the voltage readings were detected at the same time in two different digital high-resolution multimeters. The resistivity values were determined from the electrical resistance measurement taking account of the test lead distance and cross-section area of the samples.

Table 1
Characteristics of the raw powders (from H. C. Starck)

| | s.s.a. ($m^2/g$) | Grain size (μm) | Crystalline phases | Significant impurities (wt.%) | | | | | | | | |
|---|---|---|---|---|---|---|---|---|---|---|---|---|
| | | | | C | O | N | Fe | W | Si | Al | Hf | Other metals |
| $ZrB_2$ | 1. | 0.1–8 | $ZrB_2$ | 0.25 | 1.0 | 0.25 | 0.1 | | | | 0.2 | |
| $TiB_2$ | 4.0 | 0.1–4 | $TiB_2$, WC, $TiO_2$[a] | 0.14 | 2.5 | 0.19 | 0.12 | 2 | | | | 0.1 |
| $B_4C$ | 13.3 | 1.5–4.5 | $B_4C$, C[a] | | 1.7 | 0.7 | 0.05 | | 0.15 | 0.5 | | 0.1 |

[a] Traces.

Table 2
Composition, hot pressing parameters and densities of the hot pressed samples

| Sample | Composition (wt.%) | Hot pressing parameters | | | Density | |
|---|---|---|---|---|---|---|
| | | $T$ (°C) | $P$ (MPa) | Time (min) | (g/cm$^3$) | (%) |
| A | $ZrB_2$ + 4 wt.% Ni | 1850 | 30 | 30 | 6.05 | 98.0 |
| B | 55 wt.% $ZrB_2$ + 41 wt.% $TiB_2$ + 4 wt.% Ni | 1600 | 30 | 30 | 3.65 | ~100 |
| C | 83 wt.% $ZrB_2$ + 13 wt.% $B_4C$ + 4 wt.% Ni | 1870 | 30 | 10 | 5.16 | 99.6 |

Long term oxidation behaviour at 1000°C was studied in a laboratory kiln with interruptions in the tests in order to measure weight change at fixed times. Microstructure of the surface and polished cross-sections of the oxidised samples were analysed by X-ray diffraction analyses, scanning electron microscopy and EDX analyses.

## 3. Results and discussion

### 3.1. Microstructure of the hot pressed materials

Material A reached a final density of 6.05 g/cm$^3$ which is about 98% of the theoretical density. The shape and size of $ZrB_2$ grains turned out to be quite homogeneous; Ni-rich grain boundary phases were located mainly at triple points (Fig. 1a and b). It has to be pointed out that in the back scattered electron images (an example of which is shown in Fig. 1b), the contrast arises from the channelling of the accelerated electrons as a consequence of the different orientation of the $ZrB_2$ crystals and not from the change of the mean atomic number of the phases present, i.e. variations in composition and stoichiometry. From X-ray diffraction analyses, traces of $Ni_2B$ were identified and micro-analysis revealed areas containing metallic Ni with traces of oxygen as marked in Figs. 1b and 2a. Metallic nickel could not be detected on X-ray diffractograms, as its main peak is superimposed by a peak of zirconium diboride.

SIMS analyses, reported in a previous work,[36] revealed the presence of phases such as Zr–B–O, Ni–B, Zr–Ni–O in this system. These phases show some degree of reactivity between the different elements during hot pressing. Ni reacts with the $O_2$ present as an impurity in the starting $ZrB_2$ powders; subsequently, the exchange reactions with $ZrB_2$ give $Ni_2B$ and $ZrO_2$. As confirmation, small $ZrO_2$ particles were detected, mostly within $ZrB_2$ grains (Fig. 1b). Moreover, (Zr-O) compounds, probably $Zr_2O_5$,[36] were also present in the spherical inclusions distributed mainly at grain boundaries (Fig. 2a and b). The internal part of these inclusions consisted of an aggregation of small zirconium oxide particles embedded in a boron oxide-based glassy phase where zirconium, oxygen, and low amounts of impurities like Al and Si segregated, as revealed by EDX analyses. It can be hypothesised that the boron oxide-liquid phase formed at high temperature as a consequence of the

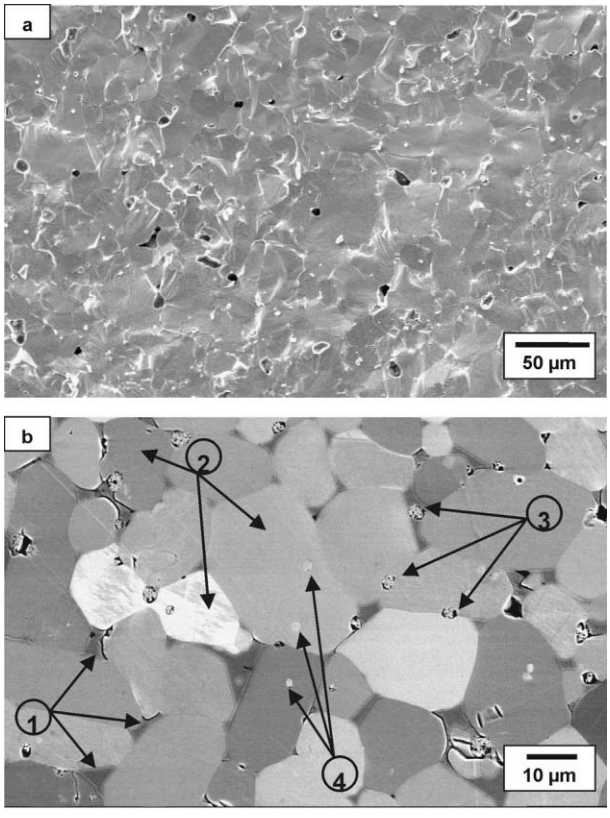


Fig. 1. (a) fracture surface of material A: $ZrB_2+4$ wt.%Ni; (b) back scattered electron image of a polished surface. The following details are marked: (1) Ni-rich grain boundary phase; (2) $ZrB_2$ grains; (3) spherical glassy inclusions; (4) $ZrO_2$ particles.

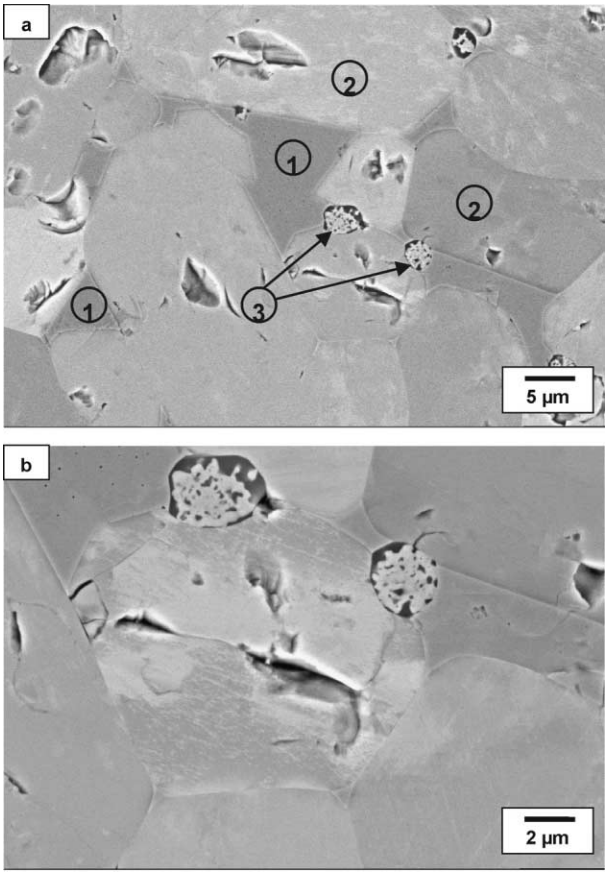


Fig. 2. Back scattered electron images of a polished section of material A. In picture a: (1) Ni-rich grain boundary phases; (2) $ZrB_2$ grains; (3) spherical glassy inclusions, containing clusters of precipitated $ZrO_2$ nanoparticles. The microstructural features are highlighted in picture (b).

concentration of oxygen and other impurities and their reaction with boron and that the glass formed during cooling from the hot pressing temperature. Zirconium oxide nanoparticles later precipitated in this glass. SIMS analyses[36] brought out two important points: (i) the presence of several $B_xO_y$ and $ZrB_xO_y$ species, indicating boron's tendency to form clusters and, (ii) the presence of other contaminants (Na, Ca, K, Cr, Ti) in addition to those indicated by the powder supplier.

The above reported results indicate that during hot pressing another melt formed, besides the Ni-based melt: a liquid glassy phase formed by $B_2O_3$ and metal cations, such as Zr and impurity elements. It is likely that a liquid film of $B_2O_3$ formed at grain boundaries due to the oxygen released from $ZrB_2$ powder particles. $B_2O_3$ melts at 723°C and vaporises at temperatures above about 800°C, but due to the applied pressure during sintering and to the fact that the liquid and vapour boron oxide-based phases were contained within closed interstitial spaces among solid particles, $B_2O_3$ could not volatilise and remained in a liquid state. Probably dewetting took place, as the liquid assumed approximately the shape of a sphere. This means that once formed, the liquid did not wet the zirconium diboride particles (depleted of the amount of the surface oxygen) and the interfacial area was reduced due to a strong driving force for shape change towards the geometrical configuration with the lowest surface energy.

The microstructural features (grain size and shape and grain boundary phases) confirmed also that the presence of Ni promoted the formation of a liquid phase at high temperature, similar to the phenomena observed during the sintering of $TiB_2$[6] and in agreement with previous results on the effects of the addition of Fe to $ZrB_2$.[7] The Ni-based liquid phase has two main effects: (i) it favours powder particle rearrangement, and (ii) enhances mass transfer mechanisms such as activated volume diffusion, surface diffusion and formation of a solid solution.[37] The temperature of this liquid phase formation, as indicated by the densification curve, is about 1260°C. Evaporation phenomena of $ZrB_2$ was also retarded due to the presence of liquid phase and enhanced grain growth was avoided. Being dependent upon the wetting behaviour, which is influenced by the surface oxidation of $ZrB_2$ particles, some residual pores which were not completely infiltrated by the liquid phase remained at the triple junctions.

Composite B, produced by the mixture $ZrB_2 + TiB_2 + Ni$, reached a density of 5.65 g/cm$^3$ which is higher than the theoretical one calculated on the basis of the starting components. This was due to the formation of (Ti, Zr)$B_2$ solid solutions as the two starting diborides are mutually and fully soluble at $T > 2000$°C.[16,38] The X-ray diffraction spectra of the crystalline phases and their relative amounts pointed out that the main part of the starting phases formed two solid solutions (Ti, Zr)$B_2$ with different volume fraction and stoichiometry (Fig. 3). On the basis of the cell parameters, two solid solutions were identified, one rich in titanium, $(Ti_{0.8}Zr_{0.2})B_2$, and the other rich in zirconium, $(Zr_{0.8}Ti_{0.2})B_2$, in amounts of 44 and 37 by vol.% respectively. Of the starting borides, an amount of about 13% of $ZrB_2$ was left, while $TiB_2$ disappeared almost completely indicating that under the adopted hot pressing conditions, the dissolution and segregation of zirconium in $TiB_2$ was favoured in comparison to the solubility of titanium in $ZrB_2$. However, a complete solution did not occur as the processing temperature of 1600°C was well below 2000°C. Additional factors, which could have influenced the rate of formation of solid solutions and their stoichiometry, were: the difference in atomic radii between Ti and Zr (Zr being about 10% larger than Ti[38]), the heating atmosphere, the cooling rate after hot pressing (slow cooling may induce decompositions[15]), the relative amounts of the starting phases, the impurities present in the starting powders, and the addition of metallic sintering aids which promote the formation of metal borides as second phases.[14,15,38] In the present case a low amount of $Ni_2B$ was actually found. Oxygen impurity leads to the formation of zirconia particles randomly distributed (Fig. 4a and b) at grain boundaries. The various phases and relative compositions are marked in the micrographs of Fig. 4a and in the EDX spectra of Fig. 4c and d. During sintering, two phenomena affect the formation and distribution of solid solutions:[38] (i) a compositional gradient in the solid solution grains, which should be limited to the grain surface for equilibrium reasons; (ii) a graded concentration of solute at triple points and within $ZrB_2$ grains, since segregation is enhanced by the different diffusion coefficients. Both these features were observed in the micrographs of Fig. 4a and b. Increased solution concentration caused lattice dilatation. These microstructural features affect the material properties. In particular, as lattice anisotropy and elastic strain

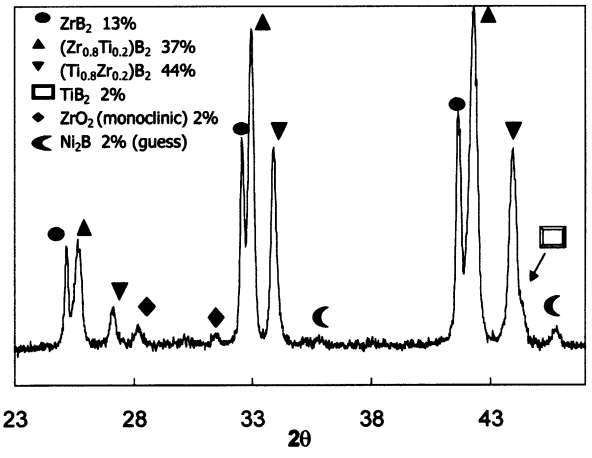


Fig. 3. X-ray diffractograms of sample B (composite $ZrB_2/TiB_2$), evidencing the formation of two different Zr–Ti–B solid solutions.

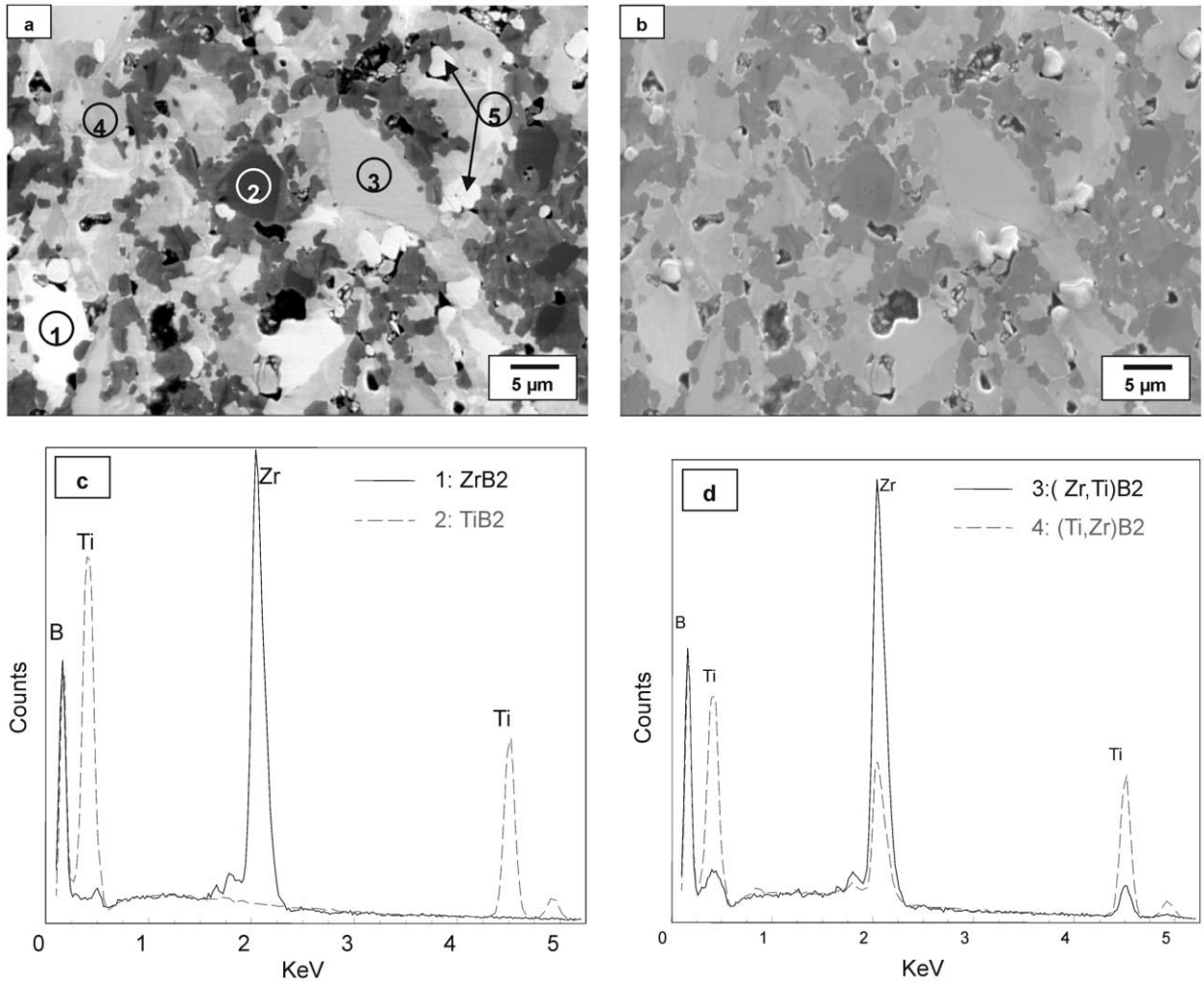


Fig. 4. (a) Back scattered electon image of a polished surface of composite B. The following phases are indicated: (1) $ZrB_2$; (2) $TiB_2$; (3) $(Zr,Ti)B_2$; (4) $(Ti, Zr)B_2$; (5) $ZrO_2$. (b) Secondary electron image of the same area represented in (a). (c) Windowless EDX spectra from the two phases indicated as 1 and 2 in picture (a). (d) Windowless EDX spectra of the two solid solutions indicated as 3 and 4 in picture (a).

energy increase in the solid solutions,[38] they determine the grain boundary cohesion in polycrystalline materials. Grain size was not homogeneous, and the material contained some defects and microcracks (Fig. 4a and b). It was not possible to confirm the amount of each phase by image analysis because the correspondence grey level-phase was disturbed by the channelling effect of the electrons.

Composite C, produced with the addition of 13 wt.% of $B_4C$ to the $ZrB_2+4$ wt.%Ni matrix material, had a final density of 5.16 g/cm$^3$ which is about the 99.6% of the theoretical density. The microstructure (Fig. 5a–c) showed $ZrB_2$ grains of 5–15 μm mixed with $B_4C$ grains of smaller dimensions (1–10 μm). The only crystalline phases revealed by X-ray diffraction analyses were $ZrB_2$ and $B_4C$. Very low amounts of Ni-based phases were only randomly found within $B_4C$ particle aggregates (Fig. 5c). Therefore, the main part of nickel introduced as sintering aids was lost during hot pressing due to two concurrent factors: (i) the relatively low dissociation energy for $B_4C$ that favoured the formation of volatile carbon oxide species and in boron (boron oxide) species, preventing also the formation of zirconia particles, (ii) the reaction between boron oxide and nickel (probably nickel oxide) that resulted in liquid phases (above about 1300°C).[40] These liquids either could have been squeezed out by the applied pressure due to their low viscosity or could have originated volatile species, being the processing temperature (1870°C) very high.

### 3.2. Mechanical properties

The mechanical properties of the three tested materials are summarised in Table 3.

#### 3.2.1. Young's modulus

This property was clearly dependent on the composition. The value measured in material A is higher than

values found in literature.[1,14,15] The addition of $TiB_2$, and the consequent formation of $(Ti,Zr)B_2$ solid solutions, decreased its value in agreement with literature data.[14–16]

### 3.2.2. Hardness

The sample with the highest value resulted the composite containing $B_4C$, however all the measured values were in the range reported in literature.[1,4,16]

### 3.2.3. Fracture toughness

The comparison of the fracture toughness values revealed the toughening effect associated with the addition of a second reinforcing phase or to a solid solution phase. In this respect, material B was tougher than material A and material C was tougher than material B. While the toughness values measured by DCM and CNB were in a very close agreement for the composite materials, the CNB value measured on material A was higher than the DCM value. As the crack pattern generated by indentation in this material (Fig. 6) is definitely far from any reasonable approximation, scarce reliability should be attributed to the data collected with this method. A direct comparison of our toughness values with those reported in literature is blurred by the different compositions and densities of the tested materials as well as the numerous models, equations and experimental parameters used to calculate the fracture toughness by DCM. The authors are not aware of any fracture toughness estimation by CNB of this kind of material.

### 3.2.4. Flexural strength

At room temperature the composite materials had a markedly higher strength than the monolithic $ZrB_2$ material (A) by virtue of their higher fracture toughness. In general the critical defects which were found as fracture origins were mainly due to processing faults, particularly the scarce homogenisation of the starting powders which resulted in aggregates or pores and voids (an example is shown in Fig. 7). At high temperature, material A showed an increase of flexural strength in the temperature range 600–800°C, reaching values higher than 600 MPa, which are excellent for this class of

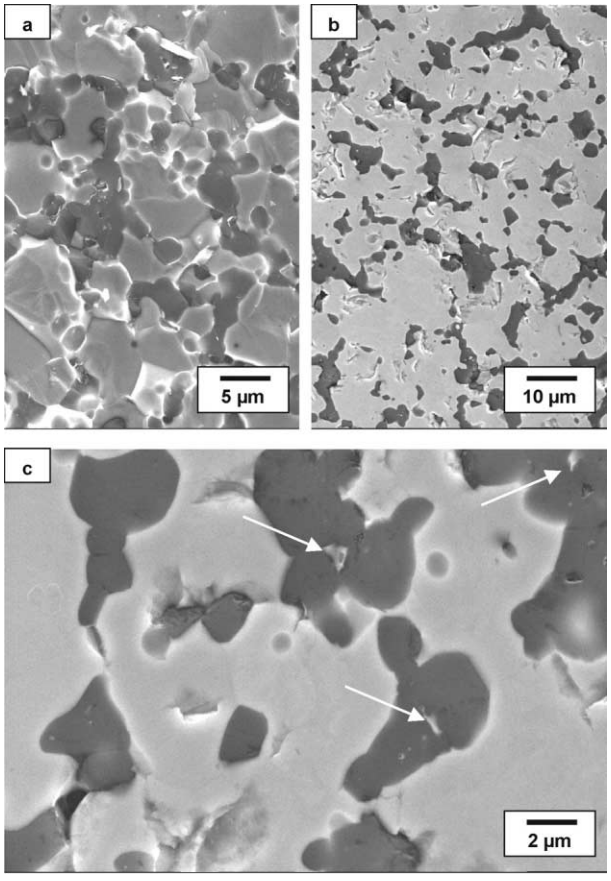


Fig. 5. Composite C. (a) Secondary electron image of the fracture surface; (b) back scattered electron image of a polished surface, evidencing the distribution of $B_4C$ particles (dark grains); (c) high magnification of polished surface: arrows indicate the presence of residual Ni-rich phases.

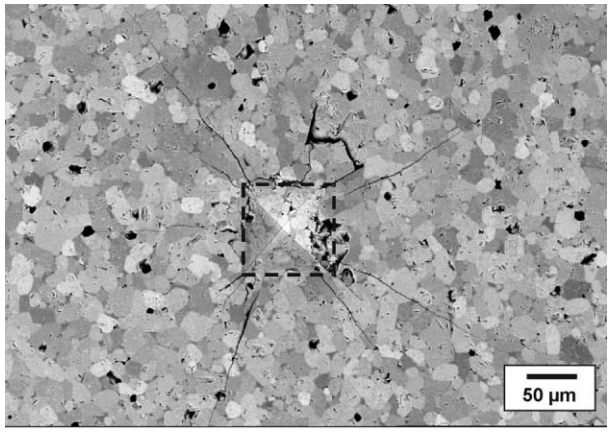


Fig. 6. Vicker's indentation on the polished surface of material A.

Table 3
Thermo-mechanical properties and electrical resistivity of the $ZrB_2$-based materials

| Sample | $\rho$ (μΩ.cm) | $E$ (GPa) | $\lambda$ ($10^{-6}$/°C) | | | $HV$ (GPa) | $K_{IC}$ (MPa$\sqrt{m}$) | | $\sigma$ (MPa) | | | |
|---|---|---|---|---|---|---|---|---|---|---|---|---|
| | | | 800 | 1000 | 1300 | | DCM | CNB | RT | 600°C | 800°C | 1000°C |
| A | 7.42 | 496 | 7.49 | 7.70 | 7.51 | 14.4±0.8 | 2.8±0.3 | 3.38±0.42 | 371±24 | 616±8 | 624±37 | 237±3 |
| B | 15.55 | 439 | 7.79 | 8.25 | 8.63 | 17.7±0.5 | 4.3±0.3 | 4.09±0.14 | 599±167 | — | 582±28 | 250±14 |
| C | 16.08 | 448 | 7.20 | 7.72 | 8.25 | 19.2±1.1 | 4.5±.3 | 4.53±0.24 | 643±86 | — | 573±99 | 148±10 |

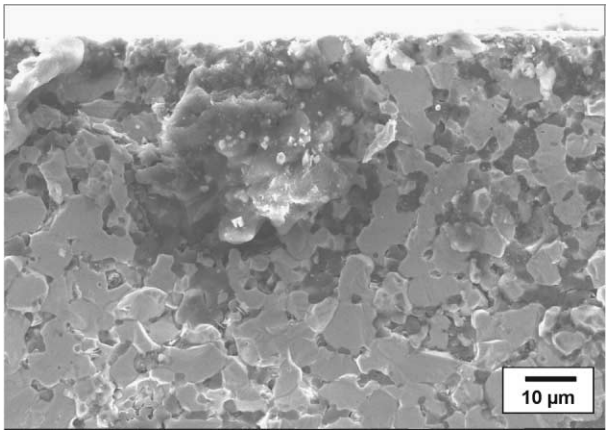


Fig. 7. Example of a crytical defect (composite C), due to either agglomerates in the raw powder or powder processing procedure.

materials, followed by a steep decrease at 1000°C. The trend for the composite materials was a slow strength degradation up to 800°C followed by a more evident drop at 1000°C. At 1000°C the load-displacement curves were markedly non-linear for all the three materials. The general high temperature behaviour of the $ZrB_2$-based ceramics can be mostly related to the characteristics of the grain boundary phase of these materials. When a metallic phase was present, as for material A, its moderate softening at intermediate temperatures was beneficial for strength. When the temperature was raised further, the excessive softening was instead detrimental for the same property. In the case of the composite materials, the grain boundary phase was unable to compensate for the natural strength degradation due to the raise in temperature.

### 3.3. Thermal expansion coefficient

The linear thermal expansion coefficient of the three materials increased with temperature (Fig. 8). In the range from room temperature to 800–1300°C, the increase for material A was from 7.5 to $7.7\times10^{-6}\ °C^{-1}$, for composite B from 7.8 to about $8.6\times10^{-6}\ °C^{-1}$ and for composite C from 7.2 to $8.3\times10^{-6}\ °C^{-1}$. Above 1300°C, an evident decrease of the thermal expansion coefficient confirmed the occurrence of the grain boundary phase softening. The thermal expansion coefficients measured for these materials were generally higher than values previously reported: $5.5\times10^{-6}\ °C^{-1}$ from room temperature up to 1000°C.[1]

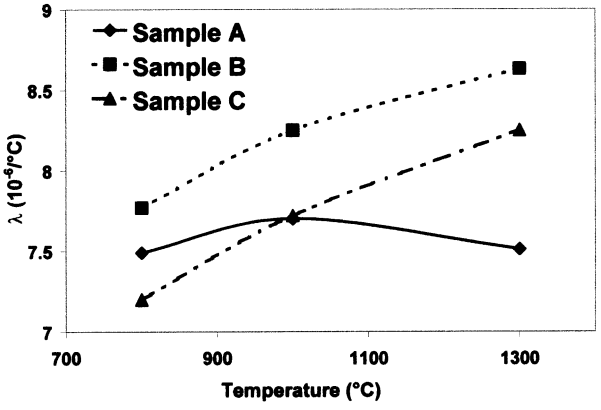


Fig. 8. Variation of the thermal expansion coefficient in function of the temperature, for the three tested materials.

### 3.4. Electrical resistivity

The electrical resistivitiy of the borides of transition metals depends on the purity and microstructural features of the materials. For a monolithic $ZrB_2$, a value of 9.2 μΩ·cm was reported.[25] In our case the presence of nickel-rich grain boundary phase lowered the resistivity to 7.4 μΩ·cm. In the composite B, the formation of $(Ti,Zr)B_2$ solid solutions increased the resistivity. The fact that $ZrB_2$ is a better conductor than $TiB_2$[25] suggests that electrical conduction in the composite of intermediate compositions may be primarily via the zirconium-rich-solid solution phase. Regarding composite C, the electrical resistivity increased, as $B_4C$ has an intrinsic resistivity of about $5\times10^{-1}$ Ω·cm.

### 3.5. Oxidation behaviour

The temperature (1000°C) selected to compare the oxidation behaviour of the two composites with that of the reference material falls in the range previously defined of rapid oxidation for $ZrB_2$,[39] during which a protective layer of crystalline $ZrO_2$ forms and the oxidation kinetics is parabolic.[33,39] The oxidation of zirconium diboride follows the reaction: $ZrB_2 + 5/2\ O_2 \rightarrow ZrO_2 + B_2O_3$, where zirconia is always a solid amorphous or crystalline product and boric oxide can be solid, fluid or gaseous, depending on the temperature.

In our case, $B_2O_3$ should have been liquid at the test temperature. Due to the presence of Ni-rich grain boundary phases and/or of additional phases in the composites, the oxidation involved more complex phenomena in comparison with those of pure $ZrB_2$.

The weight change in function of the oxidation time for the three tested materials (Fig. 9) was substantial and approximately linear up to about 40 h for the composite containing $TiB_2$. There was a weight loss for the composite containing $B_4C$. For sample A it was possible to measure the weight change only up to 24 h: longer exposure produced a complete oxidation of the test piece and the consequent fragmentation of the material.

The weight change curves reflected the contributions of two simultaneous processes. One leads to weight loss by the vaporization of volatile phases like $B_2O_3$, CO and $CO_2$, and it is supposed to occur mainly in material C. The other one promotes weight gain through the formation of $ZrO_2$, $TiO_2$, crystalline and glassy $B_2O_3$ or

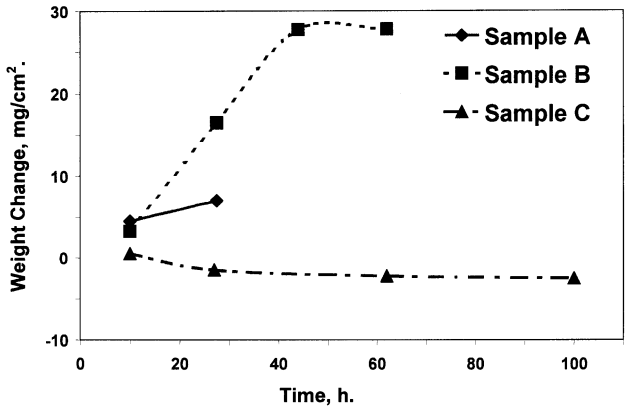


Fig. 9. Weight change due to oxidation at 1000°C of the three tested materials.

borate-based glasses and is mainly active in material B. Further additional phenomena are related to the formation of nickel oxide from the oxidation of the grain boundary phases; Ni-O species subsequently react with $B_2O_3$ causing the formation of a liquid phase according to the phase diagram $NiO.B_2O_3$.[40]

The oxidation behaviours of the three materials can be described as follows:

### 3.5.1. Material A

The only crystalline oxidation product was zirconia. The cross-section of the sample oxidised for 10 h (Fig. 10) showed that the oxidation involved both $ZrB_2$ grains and grain boundary phase. The reaction at grain boundaries was very fast; the formation of nickel oxide induced its reaction with boron oxide to liquid and solid $NiO.B_2O_3$.[40] Consequently this liquid phase progressively penetrated through the grain boundary channels towards the inner bulk. $ZrB_2$ grains, surrounded by an oxygen-rich liquid phase, underwent a fast oxidation. These phenomena led to material degradation up to the failure.

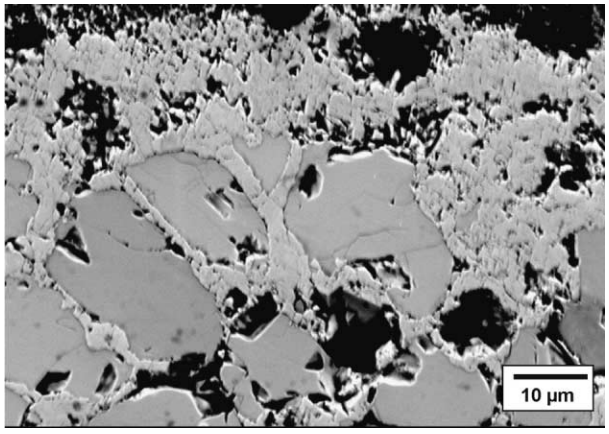


Fig. 10. Cross-section of the sample A oxidized for 10 h at 1000°C. The surface oxidation product and the reaction at grain boundaries are revealed.

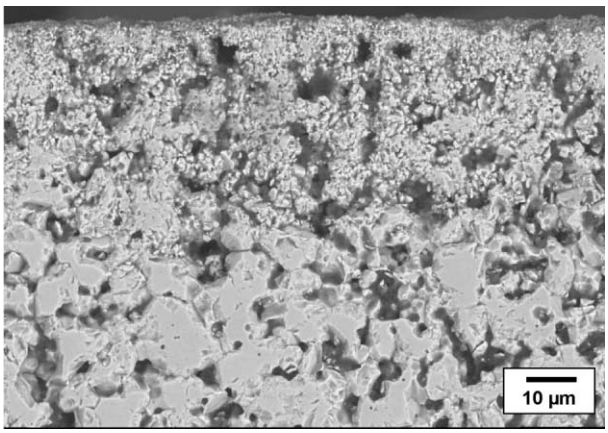


Fig. 11. Cross-section of sample C oxidized for 10 h at 1000°C. Voids due to the oxidation of $B_4C$ particles are evident.

### 3.5.2. Material B

The oxidation products were a mixture of titania, zirconia and borate-based glasses. Due to the linear kinetics observed up to 40 h of permanence at 1000°C, chemical reaction between oxygen and (Ti, Zr)$B_2$ could have been the mechanism controlling the process. During this first step the surface oxide scale was porous and allowed oxygen diffusion towards the reaction interface. Longer exposure to oxidation did not cause weight change: $B_2O_3$-based melt probably sealed the surface porosity in the oxidation product layer and protected the bulk from further oxidation.

### 3.5.3. Material C

The overall weight loss was due to the formation of volatile species: $B_2O_3$ and /or fluid glass coming from the oxidation of $ZrB_2$, of $B_4C$ and of the Ni-rich phases (although their amount is rather negligible). This material revealed the highest resistance to oxidation among the three tested materials. In fact the weight of the sample, after a slight decrease in the first period of about 30 h, was almost constant up to 100 h of exposure at 1000°C. In this regime surface reaction scale impeded further oxidation; bulk material adjacent to the reaction interface did not undergo strong degradation. The skeleton of $ZrB_2$ grains was not affected by oxidation, although $B_4C$ particles partially disappeared leaving voids (Fig. 11). One of the factors that prevented oxygen transport towards the bulk and, therefore, improved the oxidation resistance of this composite, was the quasi-absence of Ni-rich phases and their consequent fluid oxidation products along grain boundaries.

## 4. Conclusions

Dense $ZrB_2$-based composites, in the systems $ZrB_2 + TiB_2$ and $ZrB_2 + B_4C$, were produced by hot pressing. In all the compositions the addition of metallic

Ni (4 wt.%) powder promoted the formation of a liquid phase which improved mass transfer mechanisms during sintering.

From the powder mixture $ZrB_2 + TiB_2$, solid solutions Zr–Ti–B with two different stoichiometries were obtained. In the case of the other mixture, $B_4C$ particles are dispersed in the $ZrB_2$ matrix. Microstructural features are discussed in relationship with the processing parameters and starting compositions.

From the mechanical point of view the composite materials generally performed better than the monolithic $ZrB_2$ ceramic: at room temperature, the fracture toughness and the flexural strength were almost doubled. The high temperature strength behaviour was different for the monolithic and the composite materials due to the different grain boundary phase characteristics. Oxidation tests indicated that the $ZrB_2$-based composites, particularly composites containing $B_4C$ as a second phase, were more resistant to oxidation than the matrix material due the formation of surface oxide products which were protective against the complete degradation by oxidation as observed for the $ZrB_2$ matrix material.

From the technological point of view, the ability of the diborides to form solid solutions provides an opportunity to manufacture high density materials at relatively low temperature, in fact composition B reached full density at 1600°C, about 250°C lower than in the case of the other two compositions A and C.

## Acknowledgements

This project was supported by ASI (Agenzia Spaziale Italiana), Project NEIN700257.

## References

1. Morz, C., Annual mineral review. Zirconium diboride. *Am. Ceram. Soc. Bull.,* 1995, **74**(6), 165–166.
2. Low, I. M. and McPherson, R., Fabrication of new zirconium boride ceramics. *J. Mater. Sci. Lett.,* 1989, **8**, 1281–1285.
3. Upadhya, K., Yang, J. M. and Hoffmann, W.P., Materials for ultrahigh temperature structural applications. *Am. Ceram. Soc. Bull.,* 1997, **58**, 51–56.
4. Van de Goor, G., Sagesser, P. and Berroth, K., Electrically conductive ceramic composites. In *Advanced Multilayered and Fibre-Reinforced Composites*, ed. Y. M. Haddad. Kluwer Academic, The Netherlands, 1998, pp. 311–322.
5. Hayami, R., Iwasa, M. and Kinoshita, M., Effects of applied pressure on hot pressing of $ZrB_2$. *Yogyo-Kyokai-Shi,* 1987, **88**, 352–358.
6. Bellosi, A. and Monteverde, F., Microstructure and properties of titanium nitride and titanium boride-based ceramics. In *Engineering Ceramics: Multifuncional Properties-New Perspectives, Key Engineering Materials,* Vols. 175–176, ed. P. Sajgalik and Z. Lences. Trans Tech Publications, Switzerland, 2000, pp. 130–140.
7. Woo, S.-K., Han, I.-S., Kang, H.-S., Yang, J.-H. and Kim, C.-H., Sintering of zirconium diboride through Fe-based liquids phases. *J. Korean Ceram. Soc.,* 1966, **33**, 259–262.
8. Øvrebø, D. N. and Riley F. L., Densification of zirconium diboride. In *Sixth-EcerS Conference & Exhibition'', Extended Abstract*, Vol. 2. IOM Communications, University Press, Cambridge, UK, 1999, pp. 19–20.
9. Ogata, T., Mori, T., Nakamura, K., Kobaiashi, K. and Kuwajima, H., Mechanical properties of particulate dispersed and SiC whiskers reinforced boride composite materials by hot pressing. In *Advanced Structural Inorganic Composites*, ed. P. Vincenzini. Elsevier Science, Amsterdam, 1991, pp. 235–243.
10. Sorrell, C. C., Stubican, V. S. and Bradt, R. C., Mechanical properties of $ZrC/ZrB_2$ and $ZrC/TiB_2$ directionally solidified eutectics. *J. Am. Ceram. Soc.,* 1986, **69**, 317–321.
11. Sheppard, L. M., Advances in Composites processing. *Ceram. Ind.,* 1996, **146**, 72–76.
12. Cheng, Y. M. and Gadalla, A. M., Synthesis and analysis of $ZrB_2$-based composites. *Mater. Manuf. Processes,* 1996, **11**, 575–587.
13. Schuldies, J. J. and Branch, J. A., Ceramic composites: emerging processes, applications. *Ceram. Ind.,* 1992, **138**, 43–46.
14. Mroz, C., Processing and properties of microcomposite TiZrC and $TiZrB_2$ materials. *Ceram Eng. Sci. Proc.,* 1993, **14**(9-10), 725–735.
15. Mroz, C., Processing TiZrC and $TiZrB_2$. *Am. Ceram. Soc. Bull.,* 1994, **73**, 78–81.
16. Moryiama, M., Aoki, H. and Kobayashi, Y., Fabrication and mechanical properties of hot pressed $TiB_2$–$ZrB_2$ ceramic system. *J. Ceram. Soc. Jap.,* 1998, **106**(12), 1196–1200.
17. Jin, Z., Zhang, G., Bao, Y., Bai, C., Yue, X. and Zhao, H., Size effect of strengthened particles of ceramic Composites. *J. Chin. Ceram. Soc.,* 1995, **23**(6), 610–617.
18. Jimbou, R., Takahashi, K., Matsushita, Y. and Kosugi, T., SiC–$ZrB_2$ electroconductive ceramic composite. *Adv. Ceram. Mat.,* 1986, **1**, 341–346.
19. Woo, S. K., Kim, C. H. and Kang, E.S., Fabrication and microstructural evaluation of $ZrB_2$/ZrC/Zr compoisites by liquid infiltration. *J. Mater. Sci.,* 1994, **29**, 5309–5315.
20. Bundschuh, K., Schuze, M., Muller, C., Greil, P. and Heider, W., Selection of materials for use at temperatures above 1500°C in oxidizing atmospheres. *J. Eur. Ceram. Soc.,* 1998, **18**, 2389–2391.
21. Janeway, P. A., Reinforcing tomorrow's technology. *Ceram Ind.,* 1992, **138**, 42–44.
22. Breval, E. and Johnson, W. B., Microstructure of platelet reinforced ceramics prepared by the direct reaction of zirconium with boron carbide. *J. Am. Ceram. Soc.,* 1992, **75**, 2139–2145.
23. Champion, Y. and Hagege, S., Study of composite interfaces in the Zr–$ZrB_2$ system. *J. Mater. Sci. Lett.,* 1992, **11**, 290–293.
24. Jiang, D., Li, Y., Wang, J, Ma, L. and Yang, X., Study of strengthening of SiC–$ZrB_2$ multiphase ceramics. *J. Chin. Ceram. Soc.,* 1990, **18**, 123–129.
25. Rahman, M., Wang, C. C., Chen, W., Akbar, S. A. and Mroz, C., Electrical resistivity of titanium diboride and zirconium diboride. *J. Am. Ceram. Soc.,* 1995, **78**, 1380–1382.
26. Jimbou, R., Suzuki, Y. and Takahashi, K., Effect of dispersion of $ZrB_2$ on resistivity of SiC-$ZrB_2$ electroconductive ceramic composites. *J. Ceram. Soc. Jap.,* 1990, **98**, 225–230.
27. Jimbou, M. R., Suzuki, Y. and Takahashi, K., Effect of the dispersion of $ZrB_2$ on resistivity of Si-$ZrB_2$ electroconductive ceramic composites. *J. Ceram. Soc. Jpn. Inter. Ed.,* 1990, **98**, 234–239.
28. Nakamura, M., Shigematsu, I., Kanayama, K. and Hirai, Y., Surface damage in $ZrB_2$-based composite ceramics induced by electro-discharge machining. *J. Mater. Sci.,* 1991, **26**, 6078–6082.
29. Cheng, Y. M., Eubank, P. T. and Gadalla, A. M., Electrical discharge machning of $ZrB_2$-based ceramics. *Mater. Manuf. Processes,* 1996, **11**, 565–574.
30. Pankov, G. A., Fomina, G. A., Ivanov, D. A. and Val'yano, G. E., Strength and scaling resistance of a composite based on zirconium diboride. *Refractories,* 1994, **35**(9-10), 298–300.

31. Kobayashi, K., Sano, H., Maeda, K. and Uchiyama, Y., Oxidation behaviour of graphite-$B_4C$/SiC/$ZrB_2$ composite in dry and moist atmospheres. *J. Ceram. Soc. Jap. Int. Ed.,* 1992, **100**, 407–411.
32. Zhong, X. and Zhao, H., High temperature properties of refractory composites. *The Am. Ceram. Soc. Bull.,* 1999, **78**, 98–101.
33. Bellosi, A., Monteverde, F., Dalle Fabbriche, D. and Melandri, C., Microstructure and properties of $ZrB_2$-based ceramics. Submitted to *Materials Processing and Manufacturing Science*.
34. Anstis, G. R., Chantikul, P., Lawn, B. R. and Marshall, D. B., A critical evaluation of indentation techniques for measuring fracture toughness: I, direct crack measurements. *J. Am. Ceram. Soc.,* 1981, **64**, 533–538.
35. Munz, D. G., Shannon, J. L. and Bubsey, R. T., Fracture toughness calculation from maximum load in four point bend tests of chevron notch specimens. *Int. J. of Fracture,* 1980, **16**, R137–R141.
36. Daolio, S., Fabrizio, M., Piccirillo, C., Muolo, M. L., Passerone, A. and Bellosi, A., Secondary ion mass spectrometry in the characterisation of boron-based ceramics. *Rapid Commun. Mass Spectrom.,* 2001, **15**, 1–7.
37. Pastor, H., Metallic borides, preparation of solid bodies-sintering methods and properties of solid bodies. In *Boron and Refractory Borides*, ed. V. I. Matkovich. Springer, New York, 1977, pp. 457–493.
38. Zdaniewsky, W. A., Solid solubility effect on properties of titanium diboride. *J. Am. Ceram Soc.,* 1987, **70**(11), 793–797.
39. Lebugle, A. and Monte, G., Etude comparee de l'oxidation des diborured de zirconium, d'hafnium at de titane. *Rev. Int. Htes Temp. Rt Refract.,* 1974, **II**, 231–244.
40. Berkes, J. S. and White, W. B., Phase relations in the system $Li_2O.B_2O_3$–$B_2O3$-NiO. *J. Am. Ceram. Soc.,* 1969, **52**, 481–484.